Electronic Supplementary Material (ESI) for Journal of Materials Chemistry A.

Supporting Information

Methylamine lead bromide perovskite/protonated graphitic carbon nitride nanocomposites: interfacial charge carrier dynamics and photocatalysis

Ying-Chih Pu*, Hsiao-Chuan Fan, Tzu-Wei Liu and Jie-Wen Chen

Department of Materials Science, National University of Tainan, Tainan 70005, Taiwan, ROC

*E-mail**:** ycpu@mail.nutn.edu.tw

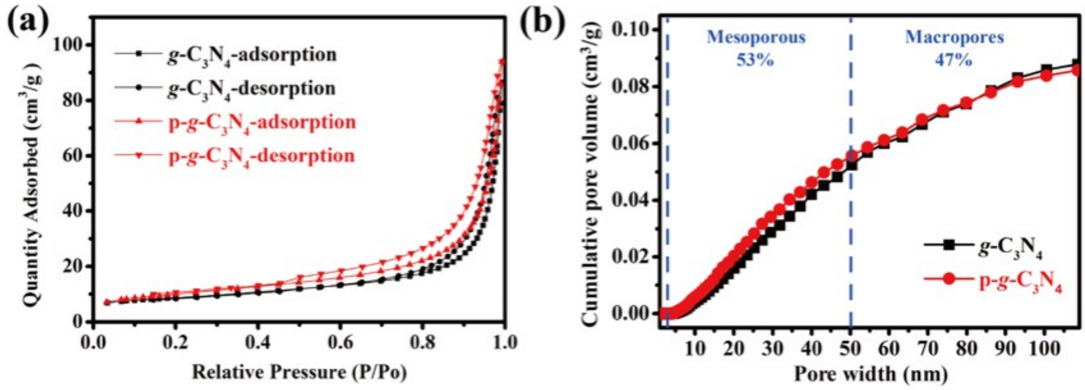

Fig. S1 (a) Nitrogen adsorption–desorption isotherms and (b) corresponding pore size distribution curves of *g*-C_3N_4 and p-*g*-C_3N_4.

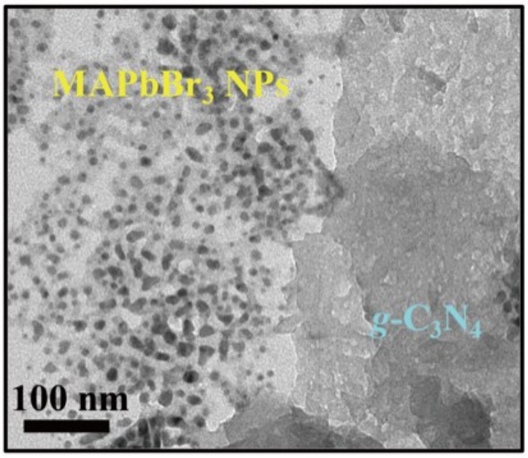

Fig. S2 TEM image of $MAPbBr_3$/*g*-C_3N_4 that was prepared by mixing *g*-C_3N_4 and precursors solution and then growth through the LARP process. The $MAPbBr_3$ NPs were observed around the edge and outside of *g*-C_3N_4 due to the weak interaction between *g*-C_3N_4 and precursor ions, MA^+, Pb^{2+}, and Br^-.

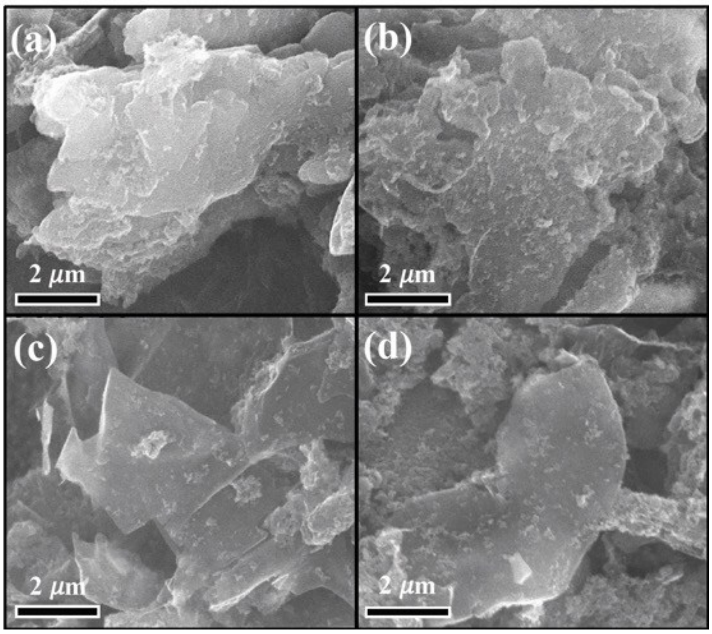

Fig. S3 SEM images of (a) p-*g*-C_3N_4, (b) $MAPbBr_3$/p-*g*-C_3N_4-0.25, (c) $MAPbBr_3$/p-*g*-C_3N_4-0.5, and (d) $MAPbBr_3$/p-*g*-C_3N_4-1.0. The significant decoration of $MAPbBr_3$ NPs on p-*g*-C_3N_4 can be observed. The decoration density of $MAPbBr_3$ NPs showed the progressively decrease as the loading amount of p-*g*-C_3N_4 increased.

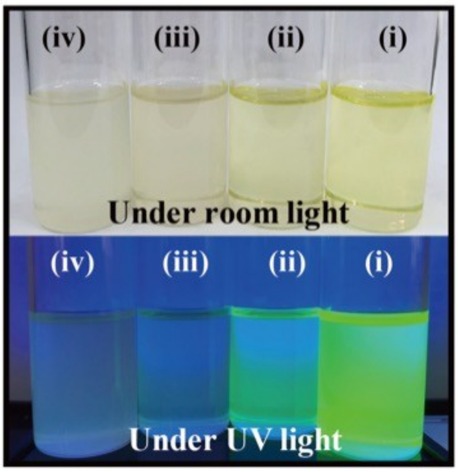

Fig. S4. Photograph of i. $MAPbBr_3$ NP and ii. $MAPbBr_3$/p-*g*-C_3N_4-0.25, iii. $MAPbBr_3$/p-*g*-C_3N_4-0.5, and iv. $MAPbBr_3$/p-*g*-C_3N_4-1.0 NCs solutions under room light and UV light (365 nm) irradiation. The progressively weaker PL emission of

MAPbBr$_3$ NPs when the incorporated amount of p-*g*-C_3N_4 was increased can be seen. Note that the concentration of MAPbBr$_3$ NPs in MAPbBr$_3$/ p-*g*-C_3N_4 NHS solutions was kept as a constant with the variation of loading amount of p-*g*-C_3N_4 to achieve the meaningful comparison of the PL intensity.

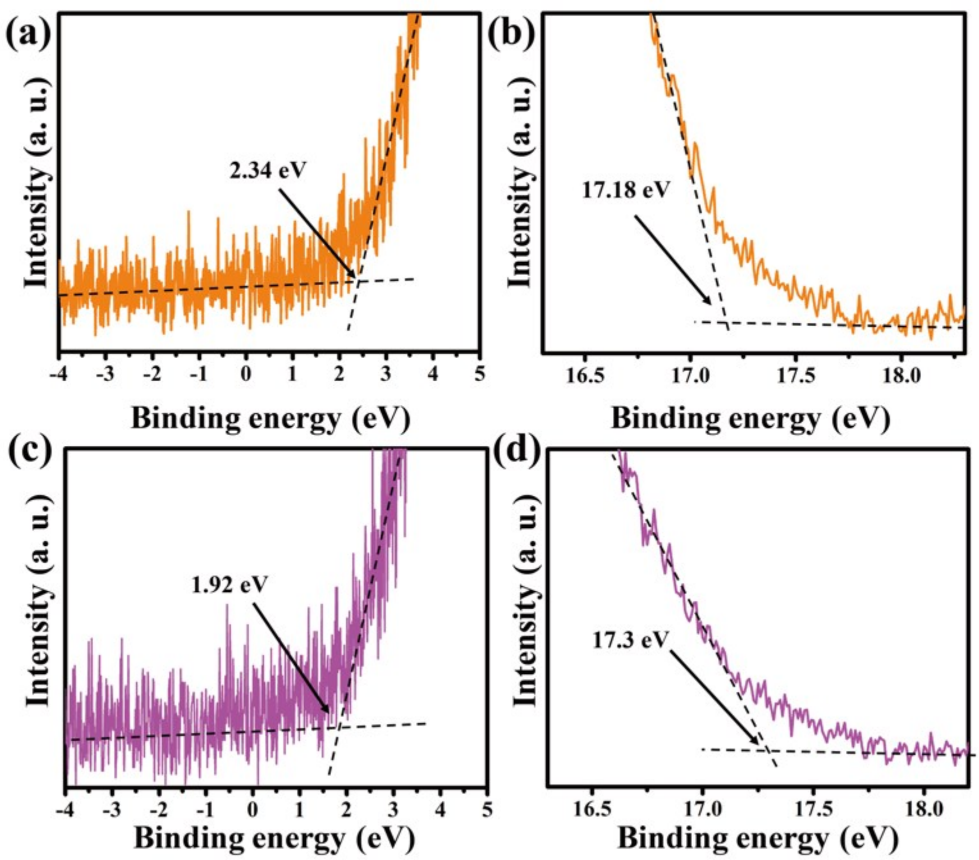

Fig. S5 UPS spectra as well as linear intersection for (a, b) p-*g*-C_3N_4 and (c, d) MAPbBr$_3$ NPs. The photoemission spectra were collected to zero point as the Fermi level, which revealed the secondary-electron cut-off energy as 17.18 and 17.3 eV for p-*g*-C_3N_4 and MAPbBr$_3$ NPs by linear extrapolation. The difference between the photon energy and the cut-off energy was calculated as the Fermi level (E_f) for the tested samples, giving -4.02 and -3.90 eV (vs. vacuum) for p-*g*-C_3N_4 and MAPbBr$_3$ NPs. On the other hand, the spectral feature close to the Fermi level represents the valence band structure of the tested samples. By the linear extrapolation along the tangent of the spectrum onset, the valence band maximum (E_{vb}) with respect to the Fermi level (E_{vb}-E_f) can be obtained as 2.34 and 1.92 eV for p-*g*-C_3N_4 and $MAPbBr_3$ NPs. Therefore, the E_{vb} of p-*g*-C_3N_4 and $MAPbBr_3$ NPs can be determined as -6.36 and -5.82 eV (vs. vacuum). Furthermore, the conduction band minimum (E_{cb}) of the p-*g*-C_3N_4 and $MAPbBr_3$ NPs can be obtained by subtracting their optical band gap (Eg) values from E_{vb}, resulting in the E_{cb} as -3.66 and -3.43 eV (vs. vacuum), respectively.

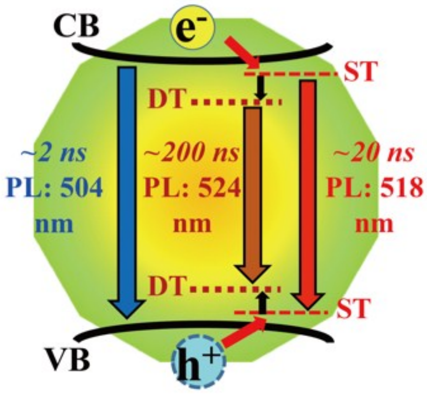

Fig. S6 Schematic illustration of the band structure and proposed assignment of lifetimes and rate constants of various charge carrier recombination and interfacial transfer processes for $MAPbBr_3$ NP. First, the photoexcited electron-hole pair in the CB and VB can be trapped into ST states and the further DT states in the time scale of ps. Senond, the remained electrons and holes in the CB and VB can recombine through a radiative pathway on the time scale of 2 ns. Last, the trapped electrons and holes in ST and DT states can also recombine through radiative processes on the time scale of 20 and 200 ns, respectively.

(a)

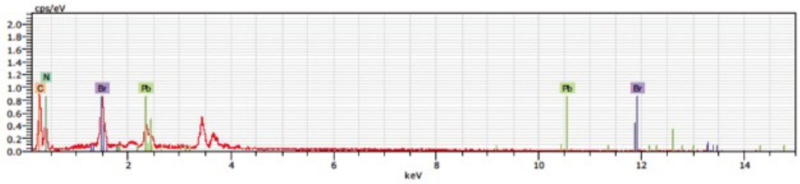

Spc0 Date:10/24/2017 11:36:05 AM HV:15.0kV Puls th.:0.78kcps

El	AN	Series	unn. C [wt.%]	norm. C [wt.%]	Atom. C [at.%]	Error (1 Sigma) [wt.%]
N	7	K-series	23.65	40.35	50.20	4.57
C	6	K-series	18.35	31.31	45.43	3.19
Br	35	L-series	8.68	14.82	3.23	0.47
Pb	82	M-series	7.92	13.52	1.14	0.36
		Total:	58.60	100.00	100.00	

(b)

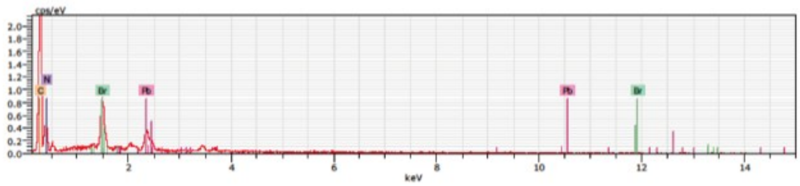

Spc0 Date:10/24/2017 11:41:31 AM HV:15.0kV Puls th.:0.78kcps

El	AN	Series	unn. C [wt.%]	norm. C [wt.%]	Atom. C [at.%]	Error (1 Sigma) [wt.%]
C	6	K-series	38.32	48.32	59.79	5.38
N	7	K-series	28.50	35.93	38.13	5.34
Br	35	L-series	6.62	8.35	1.55	0.37
Pb	82	M-series	5.87	7.40	0.53	0.28
		Total:	79.31	100.00	100.00	

(c)

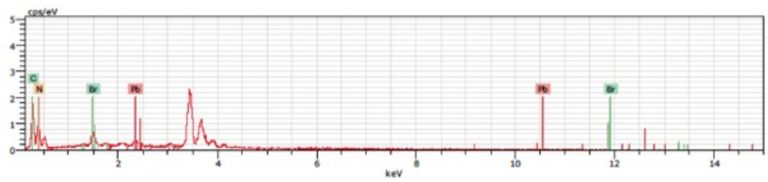

Spc0 Date:10/24/2017 11:23:07 AM HV:15.0kV Puls th.:1.85kcps

El	AN	Series	unn. C [wt.%]	norm. C [wt.%]	Atom. C [at.%]	Error (1 Sigma) [wt.%]
N	7	K-series	20.82	57.32	61.39	3.35
C	6	K-series	10.72	29.50	36.84	1.67
Br	35	L-series	2.56	7.05	1.32	0.16
Pb	82	M-series	2.22	6.12	0.44	0.12
		Total:	36.32	100.00	100.00	

Fig. S7 SEM-EDS measurement results of (a) $MAPbBr_3$/p-g-C_3N_4-0.25, (b) $MAPbBr_3$/p-g-C_3N_4-0.5, and (c) $MAPbBr_3$/p-g-C_3N_4-1.0 NCs to identify their composition. Based on the wt.% values of Pb and Br and the formula, $CH_3NH_3PbBr_3$, we can quantitatively calculate the total wt.% of $MAPbBr_3$ in $MAPbBr_3$/p-g-C_3N_4 NCs. The constitutions of $MAPbBr_3$ were 30.24, 16.80 and 14.05 wt.% in the $MAPbBr_3$/p-g-C_3N_4-0.25, $MAPbBr_3$/p-g-C_3N_4-0.5, and $MAPbBr_3$/p-g-C_3N_4-1.0 NCs, respectively.